IDENTIFICATION OF PULSE SHAPES DURING TRANSVERSE IMPACT ON COMPOSITE BEAMS AND PLATES

G. I. Rastorguev and S. I. Snisarenko

UDC 629.7:678.067

A test facility for transverse shock loading of beams and plates at small impact velocities (up to 40 km/sec) is described. The impact contact force and unsteady strains are determined for a transverse impact on fiber-layered beams and plates from fiberglass and carbon fiber-reinforced plastic. Pulse shapes are determined for various impact velocities in the range of 5–40 m/sec. *The shock loading and unsteady strain of composite beams and plates are calculated by the finite element method. The finite elements take into account transverse shears according to the Timoshenko theory and the viscoelastic material behavior according to the Voigt model.*

Key words: *composite structures, beams, plates, shock loading, unsteady strain.*

Introduction. The complexity of performing experimental studies of shock loading and unsteady deformation of composite structures consists lies in the fact that there are no clearly defined specifications on test facilities, probes, instrumentation, and test techniques. This leads to increased requirements for the accuracy and reliability of experimental data [1–8].

In experimental studies of impact processes, it is required to determine the contact force $P(t)$ upon transverse impact on plates. As is known, at velocities of shock loading of plates not exceeding 5 m/sec, the value and duration of action of the impact contact force depend on the plate stiffness, surface material, contact area, etc. (see, for example, [3, 5]). The present paper gives experimental data that allow one to identify pulse shapes for a transverse impact on composite beams and plates at various impact velocities in the range of 5–40 m/sec. Numerical calculations of the dynamic behavior of composite beams and plates at various impact velocities were performed by the finite element method using an identified contact-force function $P(t)$.

1. Test Facility for Shock Loading. The test facility used to study the unsteady deformation of beams and plates under transverse shock loading is shown in Fig. 1. The force measuring system includes a special sensor for recording the contact force, which has the shape of a cylinder made of St. 45 steel with a spherical contact surface of radius $16 \cdot 10^{-3}$ m (Fig. 2). The projectile mass can be varied in the range of $(16–200) \cdot 10^{-3}$ kg through the use of replaceable fixing screws with heads of various masses. A piezoceramic pellet is placed in the cylindrical cavity of the sensor projectile between two spherical bearings. The contact petal plates made of a brass foil $0.2 \cdot 10^{-3}$ m thick serve to provide electric contact between the guide barrel and the current-carrying surface of the tested sample (see Fig. 1), resulting in triggering of the oscillograph by the signal from the piezoceramic pellet. In the case of presence of an isolating surface, a current-carrying graphite layer is applied onto the contact zone.

In the recording of the unsteady deformation processes caused by strain wave propagation, the total root-mean-square error of the strain measurement system determined according to the developed technique [9] is 0.054 and the force measurement error is 0.061.

2. Identification of Pulse Shapes. Figure 3 shows an oscillogram of the contact force $P(t)$ for transverse central impact of a sensor projectile on a pinned fiberglass beam with a symmetric fiber netting $[0^\circ_8/\pm 45^\circ_8/90^\circ_8]$ and geometrical dimensions of $(100.0 \times 10.0 \times 10.2) \cdot 10^{-3}$ m. The impact velocity is 5 m/sec, and the projectile mass
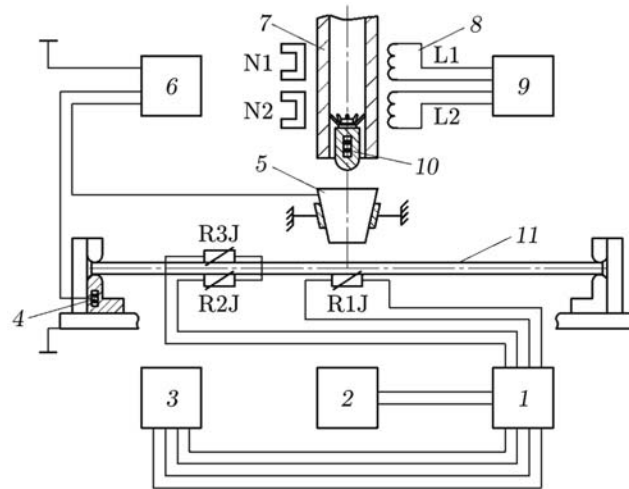
Fig. 1. Diagram of the test facility for shock loading of beams and plates: 1) high-sensitivity amplifier; 2) dynamic calibration block; 3) electronic oscillograph for recording unsteady strains; 4) piezoceramic strain sensor between spherical bearings; 5) conical contact surface; 6) electronic oscillograph for recording the impact contact force; 7) guide barrel of a light-gas gun; 8) magnetic-induction sensor for recording the projectile velocity on the base distance between magnets N1 and N2 with inductance coils L1 and L2; 9) electronic frequency meter for determining the projectile velocity; 10) piezoceramic sensor projectile; 11) test sample (beam or plate).
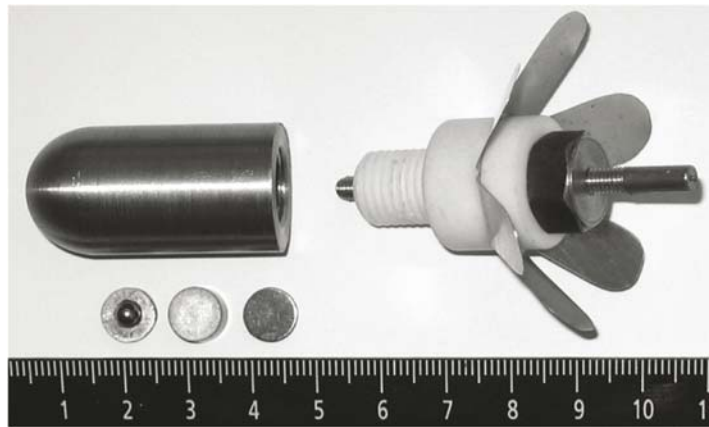

Fig. 2. Sensor recording the impact contact force.

is $51 \cdot 10^{-3}$ kg. The characteristics of the fiberglass monolayer are as follows: $\rho = 1800$ kg/m^3, $h = 0.3 \cdot 10^{-3}$ m, $E_{11} = 270 \cdot 10^8$ N/m^2, $E_{22} = 70 \cdot 10^8$ N/m^2, $G_{12} = 46 \cdot 10^8$ N/m^2, and $\nu_{12} = 0.26$. Experiments were also performed with beams of carbon fiber-reinforced plastic with the following characteristics of the monolayer: $\rho = 1450$ kg/m^3, $h = 0.125 \cdot 10^{-3}$ m, $E_{11} = 1400 \cdot 10^8$ N/m^2, $E_{22} = 85 \cdot 10^8$ N/m^2 $G_{12} = 61 \cdot 10^8$ N/m^2, and $\nu_{12} = 0.28$. The volume fraction of the polymer binder in the composite package is 35%.

As is known, at a mass ratio of the beam to projectile $m/M < 1$, a single impact takes place (see, for example, [7, 10]). At $m/M > 1$, repeated impacts occur (see Fig. 3). In the elementary theory of impact, this phenomenon can be explained as follows. At the moment of impact, the velocity of the beam exceeds the projectile velocity and the beam leads the projectile, and therefore, the density of the contact decreases, and at $t \approx 3$ μsec, a first relative maximum appears. Then, the velocity of the beam decreases and it acts as a compressing spring, and the projectile moves with the previous velocity. As a result, the density of the contact increases, and at $t \approx 19$ μsec, a second maximum appears. After that, the projectile moves in the opposite direction, and at $t \approx 86$ μsec, a rebound occurs.
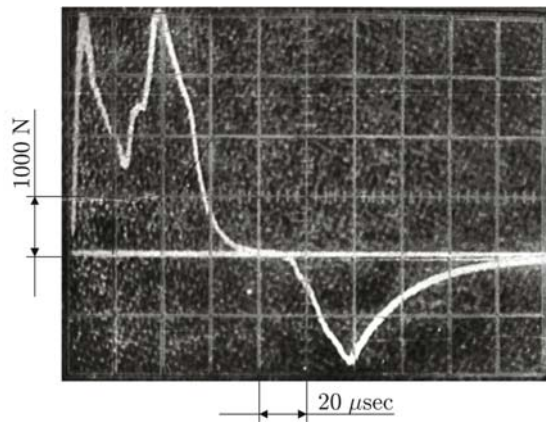
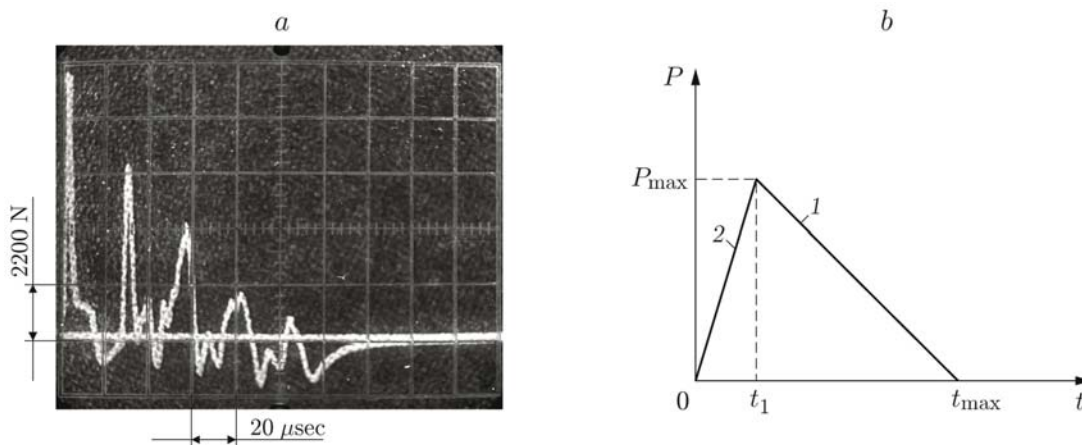Fig. 3. Oscillogram of the contact force $P(t)$ for a transverse central impact on a pinned fiberglass beam.

Fig. 4. Oscillogram of the contact force $P(t)$ (a) and pulse shape (b) for a transverse central impact on a rigidly fixed fiberglass plate: segment 1 refers to $P = P_{max}(1 - t/t_{max})$ and segment 2 to $P = P_{max}t/t_1$.

For numerical calculations, it is necessary to approximate the time dependence of the contact force $P(t)$ by specified functions. In [5, pp. 8–46; 11] and others, it is noted that for low-velocity (less than 5 m/sec) shock loading of plates, the contact force can be well approximated by a sinusoidal half-wave with the maximum amplitude P_{max} and duration t_{max}. The experiments performed in the present work show that, at impact velocities of 5–40 m/sec, other approximations are required.

Figure 4a gives an oscillogram of the contact force $P(t)$ for a transverse central impact on a rigidly fixed fiberglass plate with fiber stacking angles of $[0_8^\circ/\pm 45_8^\circ/90_8^\circ]$ and geometrical dimensions of $(100.0 \times 100.0 \times 7.2) \times 10^{-3}$ m. The impact velocity is 18 m/sec, and the projectile mass is $51 \cdot 10^{-3}$ kg. The pulse envelope for repeated impacts is a triangle with increasing and decreasing regions (Fig. 4b). The number of repeated impacts increases with increasing shock loading velocity. This shape of the pulse envelope is retained at impact velocities of 5–40 m/sec, with the length of the initial region of increasing load being much smaller than the length of the region of decreasing load. In addition, the length of the initial region is smaller the higher the impact velocity. At impact velocities higher than 40 m/sec up to the penetration velocity, failure of the plate should be expected on the ascending branch of the pulse (see Fig. 4b); therefore, in this case, the contact force should be approximated by a triangular pulse of only increasing load.

For a transverse impact on carbon fiber-reinforced plastic plates, the maximum force P_{max} and the time of its action t_{max} are different. Therefore, we performed experiments on shock loading of plates of composites consisting of fiberglass and carbon fiber-reinforced plastic layers with fiber stacking angles of $[0_8^\circ/\pm 45_8^\circ/90_8^\circ]$ and geometrical
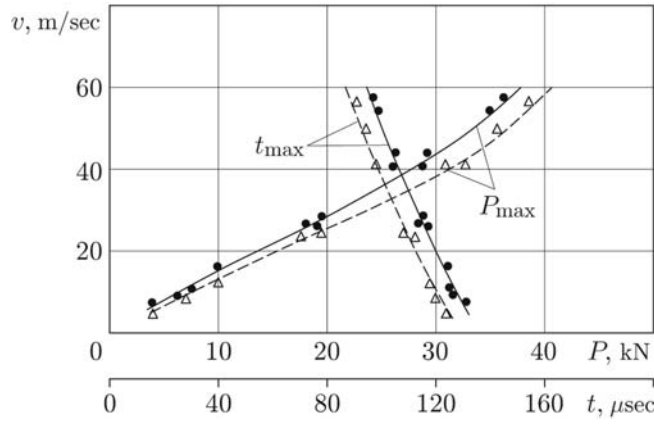
1022

Fig. 5. Maximum values of the contact force $P_{\max}$ and durations of its action $t_{\max}$ for an impact on a rigidly fixed plate of a composite consisting of layers of fiberglass and carbon fiber-reinforced plastic at various impact velocities: solid curves refer to an impact on fiberglass, and dashed curves to an impact on carbon fiber-reinforced plastic; curves correspond to calculation results, and points to experimental data.

dimensions of $(100.0 \times 100.0 \times 10.2) \cdot 10^{-3}$ m at various shock loading velocities; the results of the experiments are presented in Fig. 5. Impact was implemented on the same plate (on both carbon fiber-reinforced plastic and fiberglass) by a projectile of mass $51 \cdot 10^{-3}$ kg. It was found that for impact from fiberglass at impact velocities of 5–40 m/sec, the maximum values of the impact force $P_{\max}$ are approximately 15% smaller and the time of complete loss of contact $t_{\max}$ is approximately 10% larger than those for impact on carbon fiber-reinforced plastic. In this case, lower strains and stresses arise in the hybrid composite plate. Thus, using fiberglass as a protective face layer for carbon fiber-reinforced plastic plates increases its shock resistance to a low-velocity impact at impact velocities of 5–40 m/sec. Under high-velocity (more than 200 m/sec) shock loading, the indicated effect is enhanced due to a loss of the kinetic energy of the projectile and its expenditure in plate deformation during penetration (see, for example, [1, pp. 50–92, 391–483]).

3. Numerical Study of Unsteady Strains. Calculations of unsteady strains under the action of the impact force functions $P(t)$ determined in the present work were performed for composite beams using the finite element method (FEM). The equation of motion of the FEM is written as

$$[M]\{\ddot{\delta}\} + [C]\{\dot{\delta}\} + [K]\{\delta\} = P(t)\{\delta_j\}, \tag{1}$$

where $[M]$, $[C]$, and $[K]$ are the mass, viscosity, and stiffness matrices, respectively; $\{\delta\}$ is the vector of generalized displacements, $P(t)$ is a function of the impact contact force, and $\{\delta_j\}$ is the Kronecker symbol. Integration of the equation of motion of the FEM (1) is performed by Runge–Kutta method.

The finite elements took into account transverse shears according to the Timoshenko theory proposed in [12]. For the multilayered fiber beam, a third-order finite element with two nodal points and four generalized displacements at the node was chosen:

$$\{\delta^e\}^{\mathrm{t}} = \{w_0, w_0', \gamma_0, \gamma_0', w_1, w_1', \gamma_1, \gamma_1'\}.$$

Here w_0 and w_1 are deflections and γ_0, γ_1 are rotations.

As the rheological model of the mechanical behavior of composite materials we used the linear dependence of stresses $\{\sigma\}$ on strains $\{\varepsilon\}$ and strain rates (Voigt model)

$$\{\sigma\} = [D]\{\varepsilon\} + [W]\{\dot{\varepsilon}\},$$

where $[D]$, $[W]$ are the reduced stiffness and viscosity matrices of the composite material.

Figure 6 gives calculated maximum bending ε_{b} and shear $\varepsilon_{\mathrm{sh}}$ strains for flight of pinned carbon fiber-reinforced plastic beams with fibers stacking angles of $[0_8^\circ/\pm 45_8^\circ/90_8^\circ]$ and in geometrical dimensions of $(250 \times 10 \times 10) \cdot 10^{-3}$ m. The beam was loaded by a central transverse sinusoidal pulse with the maximum value of the impact force $P_{\max} = 2 \cdot 10^3$ N and the time of its action $t_{\max} = 2 \cdot 10^{-4}$ sec, which corresponds to collision of the beam and projectile of mass $51 \cdot 10^{-3}$ kg at a velocity of 5 m/sec. Points show the maximum experimental bending strains
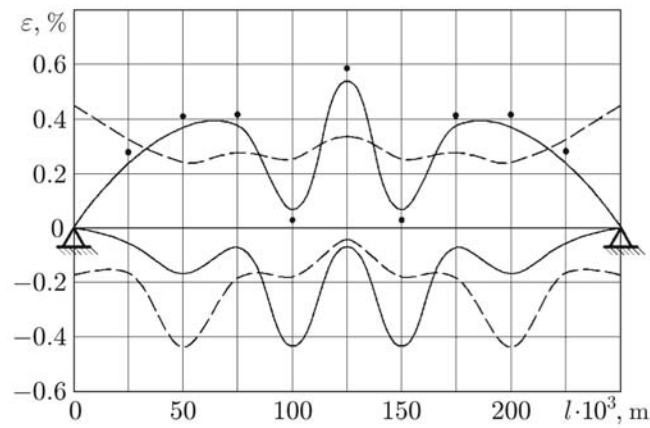
Fig. 6. Maximum bending ε_{b} (solid curves) and shear $\varepsilon_{\mathrm{sh}}$ (dashed curves) strains for flight of a carbon fiber-reinforced plastic beam loaded by a central transverse sinusoidal pulse: curves correspond to calculation results, and points to experimental data.
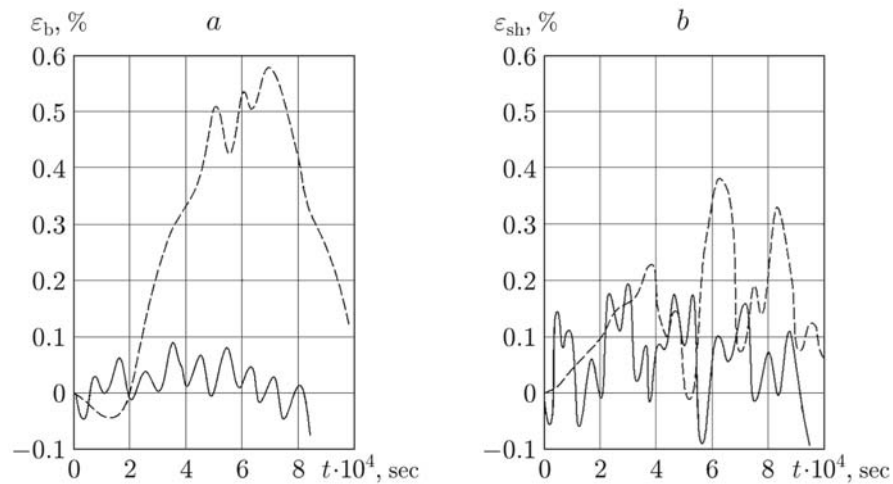

Fig. 7. Time dependences of the unsteady bending (a) and shear (b) strains of a carbon fiber-reinforced plastic beam loaded by a central transverse triangular pulse ($P_{\max} = 2 \cdot 10^3$ N): solid and dashed curves correspond to $t_{\max} = 25 \cdot 10^{-6}$ and $400 \cdot 10^{-6}$ sec, respectively.

obtained by the KF-4P1-5-100-B-12 strain sensors R2J and R3J (see Fig. 1) and an S8-13 electronic oscillograph. The R1J strain sensor synchronized the moment of oscillograph triggering with the moment the bending wave acted on the strain sensors R2J or R3J. The symmetric arrangement of the strain sensors R2J and R3J eliminates longitudinal strains during transverse shock loading and unsteady deformation of plates. The difference between the calculated and experimental values does not exceed 10%.

A characteristic feature of the unsteady deformation of beams made of fiber-layered materials such as fiber-glass and carbon fiber-reinforced plastic, which have low shear stiffness is that the bending and shear strains are of the same order of magnitude. The calculations show (see Fig. 6) that the maximum unsteady bending strains at the center of the beam is equal to $\varepsilon_{\mathrm{b}} = 0.565\%$, and the maximum shear strain is $\varepsilon_{\mathrm{sh}} = 0.432\%$. Thus, for low-velocity (less than 5 m/sec) shock loading of beams with ratios of the height h in cross section to the length L in the range of $0.04 < h/L < 0.10$ the shear strains are of the same order of magnitude as the bending strains ($\varepsilon_{\mathrm{sh}}/\varepsilon_{\mathrm{b}} \approx 0.8$–$0.9$). For short beams with a ratio $h/L > 0.1$, fracture should be expected as a result of shear strains because, in this case, they are larger than the bending strains ($\varepsilon_{\mathrm{sh}}/\varepsilon_{\mathrm{b}} \approx 1.06$). At a shock loading velocity exceeding 5 m/sec, as the time of action of the impact contact force decreases, the fracture due to shear strains can also occur in the case of longer beams with a ratio $h/L < 0.04$. This result coincides with the results obtained in [13].

1024

As shown in the present work, as the shock loading velocity increases in the range of 5–40 m/sec up to the penetration velocity, the impact contact force pulses have a nearly triangular shape with the maximum amplitude $P_{\max}$ and duration $t_{\max}$. Figure 7 shows calculated unsteady bending $\varepsilon_{\mathrm{b}}(t)$ and shear $\varepsilon_{\mathrm{sh}}(t)$ strains of a pinned carbon fiber-reinforced plastic beam with fiber stacking angles of $[0_8^\circ/\pm 45_8^\circ/90_8^\circ]$ and geometrical dimensions of $(250 \times 10 \times 10) \cdot 10^{-3}$ m in the section at the distance $x = L/5$ from the point of application of a central transverse triangular pulse at $t_{\max}/t_1 = 10$ (see Fig. 4b). For an impact pulse duration $t_{\max} = 400 \cdot 10^{-6}$ sec (dashed curve in Fig. 7a), the maximum unsteady bending strains are larger than the maximum shear strains (dashed curve in Fig. 7b). As the pulse duration decreases to $t_{\max} = 25 \cdot 10^{-6}$, the ratio between the bending and shear strains changes: the bending strains (solid curve in Fig. 7a) become smaller than the shear strains (solid curve in Fig. 7b).

Thus, using dependences of the identified functions of the impact force on impact velocities in numerical studies of unsteady deformation allows one not only to improve the calculation accuracy but also to determine the fracture pattern of composite structures.

Conclusions. The analysis of the experimental results on the contact force under transverse impact on composite beams and plates as a function of the shock loading velocity and results of numerical calculations of unsteady deformation leads to the following conclusions.

For transverse shock loading of composite beams and plates, the contact force depends on the shock loading velocity. In a low-velocity (less than 5 km/sec) impact, the pulse shape is nearly sinusoidal with the maximum amplitude $P_{\max}$ and duration $t_{\max}$. At impact velocities of 5–40 m/sec, the pulse shapes can be approximated by a triangular pulse with increasing and decreasing regions.

For bearing structures of carbon fiber-reinforced plastic, use of face coatings of fiberglass under shock loading conditions leads to a decrease in its intensity to 15% and, hence, to an increase in the shock stability of the structure as a whole.

REFERENCES

1. A. V. Gerasimov (ed.), *Theoretical and Experimental Studies of High-Velocity Interaction of Bodies* [in Russian], Tomsk State University, Tomsk (2007).
2. N. A. Abrosimov and V. G. Bazhenov, *Nonlinear Problems of Dynamics of Composite Structures* [in Russian], Nizny Novgorod State University, Nizny Novgorod (2002).
3. V. M. Fomin, A. I. Gulidov, G. A. Sapozhnikov, et al., *High-Velocity Interaction of Bodies* [in Russian], Izd. Sib. Otd. Ross. Akad. Nauk, Novosibirsk (1999).
4. A. V. Karmishin, A. I. Zhukov, V. G. Kolosov, et al., *Methods of Dynamic Calculations and Tests of Thin-Walled Structures* [in Russian], Mashinostroenie, Moscow (1990).
5. S. S. Grigoryan, *Impact Dynamics* [in Russian], Mir, Moscow (1985).
6. W. Goldsmith, *Impact: the Theory and Physical Behavior of Colliding Solids,* Dover, New York (2001).
7. E. G. Goloskokov and A. P. Filippov, *Unsteady Vibrations* [in Russian], Naukova Dumka, Kiev (1977).
8. N. A. Kil'chevskii, *Dynamic Contact Compression of Solids: Impact* [in Russian], Naukova Dumka, Kiev (1976).
9. S. M. Kokoshvili, *Methods of Dynamic Tests of Rigid Polymer Materials* [in Russian], Zinatne, Riga (1978).
10. S. P. Timoshenko, *Vibration Problems in Engineering*, Van Nostrand, Toronto–New York–London (1955).
11. M. Yener and E. Wolcott, "Damage assessment analysis of composite pressure vessels subjected to random impact loading," *J. Appl. Mech.*, **11**, 124–129 (1989).
12. R. B. Rikards, *Finite Element Method in the Theory of Shells and Plates* [in Russian], Zinatne, Riga (1988).
13. A. E. Bogdanovich, *Nonlinear Problems of the Dynamics of Cylindrical Shells* [in Russian], Zinatne, Riga (1987).